

Hydrological response of weathered clay-shale slopes: water infiltration monitoring with time-lapse electrical resistivity tomography

J. Travelletti,^{1,2*} P. Sailhac,¹ J.-P. Malet,¹ G. Grandjean³ and J. Ponton¹

¹ Institut de Physique du Globe de Strasbourg, CNRS UMR 7516, University of Strasbourg, 5 rue René Descartes, 67084 Strasbourg Cedex, France

² GEOPHEN - LETG, CNRS UMR 6554, University of Caen Basse-Normandie, Caen, France

³ BRGM, Bureau des Recherches Géologiques et Minières, Orléans, France

Abstract:

This work presents an attempt to monitor water infiltration and subsurface flow within a clay-shale landslide using time-lapse electrical resistivity tomography (ERT). A rainfall experiment was carried out on a plot of 100 m² at the Laval landslide in the Draix experimental catchments (ORE Draix, South French Alps) in order to characterize the spatial and temporal development of water circulation in the soil and to identify when steady-state flow conditions are reached. The experiment was conducted during 67 h with initial unsaturated conditions in the slope. The apparent electrical resistivity values were inverted with a time-lapse approach using several cross models. The results indicate a significant decrease in resistivity (−18%) compared to the initial state in the rain plot. Downslope progression of negative resistivity anomalies is imaged suggesting that vertical and subsurface lateral flows have developed. About 21 h after the start of the rain experiment, a constant level of resistivity values is observed indicating that the hydrological system reached steady-state flow conditions. This observation is consistent with ground water level observations and chemical tracer analysis. Computed differences in time of steady-state conditions highlight possible preferential flows near the landslide toe. A hydrological concept of functioning of the slope is proposed, and apparent saturated hydraulic conductivity (K_s of $1.7 \times 10^{-4} \text{ m} \times \text{s}^{-1}$) is computed from the steady-state times. This study demonstrates the potentiality of ERT monitoring to monitor water infiltration in clay-shale slopes and the high water transfer capacity of reworked clay-shale material. Copyright © 2011 John Wiley & Sons, Ltd.

KEY WORDS water infiltration; geophysical monitoring; steady-state flow; electrical resistivity tomography; landslide

Received 10 July 2010; Accepted 13 December 2010

INTRODUCTION

The badland landscape observed in the Jurassic clay-shale (e.g. black marls) catchments of the South French Alps is the result of the conjunction of favourable lithologic and climatic factors. Freeze–thaw and wetting–drying cycles progressively disintegrate the black marls formation thus favouring the annual development of a weathered marls layer exposed to surface runoff erosion and shallow landslides (Antoine *et al.*, 1995; Maquaire *et al.*, 2003; Mathys *et al.*, 2003a). The weathered marls can be mobilized by Hortonian runoffs especially during high-intensity rainfalls in summer. This causes flash floods and hyperconcentrated flows inducing significant problems in sedimentation reservoirs and river systems (Oostwoud Wijdenes and Ergenzinger, 1998; Descroix and Olivry, 2002). Saturation of the weathered marl layers can also locally trigger shallow landslides supplying high sediment loads to the basins. In addition, rain infiltration in the fractured marls bedrock contributes to the triggering of larger landslides whose geometry is controlled by the bedding and the discontinuities (Maquaire

et al., 2003; Malet *et al.*, 2011). To characterize the water transfer capacity and identify the main hydrological processes occurring in these slopes, several studies have been undertaken (Corona *et al.*, 2002; Mathys *et al.*, 2003b; Estèves *et al.*, 2005). From these analyses, slope gradient, soil surface characteristics and initial soil moisture conditions are the main factors controlling surface runoff and subsurface flow patterns. Cras *et al.* (2007) highlighted the global control exerted by subsurface water flow in the triggering of flash floods after wet pre-event conditions with water contribution of up to 20% at the peak discharge. However, little is known about the spatial and temporal development of subsurface water flow in this type of reworked clay-shale soils, especially at the time when the maximal storage capacity is reached. This time corresponds to a threshold value indicating when subsurface flow rates become maximal for specific rainfall patterns and initial soil hydrological conditions.

To characterize the dynamics of water infiltration, a rainfall experiment was undertaken in October 2007 at the Laval landslide (Laval catchment, ORE, Draix, South French Alps; Figure 1A). A multi-technique approach was set up to monitor soil deformation (DGPS, terrestrial laser scanning) and soil hydrology [e.g. groundwater level measurements, soil water content monitoring, chemical

*Correspondence to: J. Travelletti, Institut de Physique du Globe de Strasbourg, CNRS UMR 7516, University of Strasbourg, 5 rue René Descartes, 67084 Strasbourg Cedex, France.
E-mail: julien.travelletti@unistra.fr

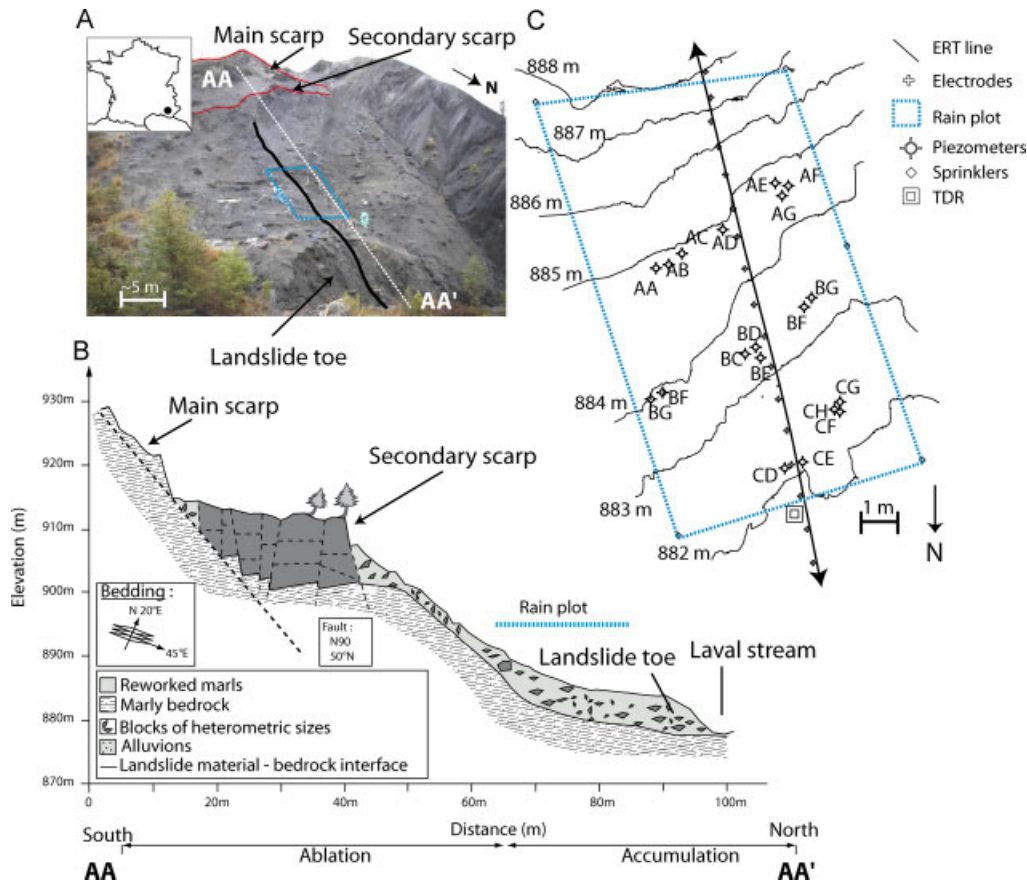


Figure 1. (A) Photograph of the Laval landslide. The rain experiment plot and the location of the ERT line are detailed. (B) Cross section of the landslide (modified from Fressard *et al.*, 2009). (C) Monitoring equipment installed on the rain plot

tracer analysis, seismic tomography and electrical resistivity tomography (ERT)]. Grandjean *et al.* (2009) used a fuzzy set theory in order to combine the ERT and the seismic information to provide a first qualitative interpretation of water movement in the soil. This article presents an analysis of water movement based on the interpretation of ERT monitoring using a time-lapse inversion approach. The objectives are: (i) to characterize the spatial and temporal development of the water infiltration front and the subsurface flow in the soil and (ii) to identify the time when the conditions of steady-state flow (e.g. constant water flow rate) is reached.

Six inverted models of time-lapse inversion are used to estimate the uncertainties of the resistivity values and to select the most appropriate inverted model for the hydrological interpretation. The best model has been chosen according to the root mean square error (RMS) of the inversion and the stability of the resistivity values in a test area where no change in resistivity is expected. The noise level due to temperature changes in the inversion process is estimated. A method for determining the time of steady-state flow conditions is proposed and this time is compared to hydrological measurements. A hydrological concept of functioning of the slope is proposed. Finally, the limitations of ERT monitoring to estimate soil water contents and the possibility of deriving apparent saturated hydraulic conductivity values are discussed.

INVESTIGATED AREA: THE LAVAL LANDSLIDE

The Laval landslide is located in the Draix experimental catchments (ORE Draix, south French Alps) characterized by Mediterranean and mountain climate influences (annual average of precipitation and temperature of 900 mm and 10.9 °C over the period 1970–2000) and unsaturated slope conditions within most part of the year (Mathys *et al.*, 2003a) (Figure 1A and B).

The Laval landslide was triggered in January 1998 and extended over an area of 4000 m² from 875 to 935 m elevation (average slope of 32°). The total volume of the accumulation zone is estimated at 8000–10 000 m³ (Fressard *et al.*, 2009). The toe of the landslide is regularly eroded by the Laval stream.

The landslide material is composed of weathered Callovo-Oxfordian black marls characterized by a heterogeneous fabric of flakes and centimetric to decimetric blocks encased in a sandy-silty matrix. The landslide thickness was determined from several dynamic penetration tests and geophysical prospecting (seismic and ERT tomographies) and varies between 1 and 6 m (Fressard *et al.*, 2009; Grandjean *et al.*, 2009) (Figure 1B).

Soil characteristics were determined in the laboratory on undisturbed samples (Garel *et al.*, 2011). The porosity of the matrix (determined with volumetric soil samplings) varies between 0.38 and 0.52, while the porosity of intact blocks of marls varies between 0.17 and 0.23.

The saturated hydraulic conductivity (K_{sat}) was measured with a steady head permeameter, and varies between $1.1 \times 10^{-3} \text{ m s}^{-1}$ for the matrix and $3.0 \times 10^{-6} \text{ m s}^{-1}$ to $7.5 \times 10^{-5} \text{ m s}^{-1}$ for the intact blocks according to the orientation of the schistosity (Malet *et al.*, 2003).

METHODS

Simulated rain experiments

The experimental rain plot is located in the accumulation zone of the Laval landslide (Figure 1A–C) on a moderate slope gradient (*ca* 20°); the zone is characterized by macro-fissures at the surface which may act as possible preferential water pathways (Garel *et al.*, 2011). The simulated rainfall was applied on an area of 100 m^2 with an average intensity of 11 mm h^{-1} during 67 h and simulated using a water pump and six sprinklers located along the borders of the experimental plot (Figure 1C). Chemical tracers (chlorure, bromure) were added to the rain water to characterize the water pathways and flow velocity. The electrical resistivity of the rain was kept constant ($18 \pm 4 \text{ } \Omega\text{m}$) during all the experiment. A network of shallow piezometers (with varying depths of 1–4 m) were installed for water sampling and ground-water level observations.

The rain experiment started with unsaturated hydrological condition in the slope material (initial saturation degree of *ca* 27%). The resistivity of the pre-event water present in the slope has an average resistivity of $5 \pm 3 \text{ } \Omega\text{m}$; its spatial distribution inside the area is heterogeneous. As convention in this study, the rain experiment starts at the time t_0 .

More detailed information on the rain experimental set-up and on the hydrological observations can be found in Garel *et al.* (2011).

Electrical resistivity tomography

ERT is very sensitive to subsurface changes in water saturation and pore water salinity. The method is potentially able to provide a better spatial characterization of water flows within a slope than local point measurements such as tensiometry or time-domain reflectometry (Daily *et al.*, 1992; Binley *et al.*, 1996; Barker and Moore, 1998; Olsen *et al.*, 1999; Slater *et al.*, 2000; French and Binley, 2004). Therefore, this technique is widely used to complement classical hydrological methods (Robinson *et al.*, 2008). The high sensitivity to subsurface geoelectrical structures makes also ERT particularly interesting for estimating bedrock geometry in landslide investigations when a resistivity contrast between the bedrock and the mobilized mass exists (Jongmans and Garambois, 2007; Marescot *et al.*, 2008).

The resistivity values are not directly obtained from surface-based ERT surveys. Electrode spacing, electrical current intensity and electrical potential are the measured parameters used to calculate apparent resistivity values which are then inverted to estimate the true resistivity values (Samouëlian *et al.*, 2005; Rings and Hauk, 2009).

Several inverted models can be calculated for the same set of apparent resistivity values. Consequently, the inversion cannot be very precise and non-uniqueness of the solution can lead to misinterpretation (Olayinka and Yaramanci, 2000). Therefore, several inverted models should be calculated for the same dataset thus giving an estimation of the inverted resistivity accuracy (Nguyen and Kemna, 2005).

Quantitative interpretation of ERT data is difficult in clay-rich soils due to the influence on conductivity along clay surfaces and solute concentration on the bulk soil conductivity (Glover *et al.*, 2000). Petrophysical relationships based on the modified Archie's law (Archie, 1942) take into account these influences on the bulk conductivity obtained from ERT (Waxman and Smits, 1968; Sen *et al.*, 1988; Glover *et al.*, 2000; Shah *et al.*, 2005). However, petrophysical parameters are often difficult to measure because of the geological variability (e.g. sedimentary and structural changes). As a consequence, many studies usually assume a unique petrophysical relationship with negligible or constant conductivity along clay surfaces (French *et al.*, 2002; Winship *et al.*, 2006). For temporal monitoring of water infiltration, differences between resistivity measurements are generally more accurate than absolute values (Samouëlian *et al.*, 2005). Therefore, resistivity anomalies are often determined in relation to a set of measurements realized before the start of the experiment to describe the initial state.

The ERT is located in the central part of the experimental plot in the direction of the main slope gradient (Figure 1A and C), and the centre of the ERT line coincides with the centre of the experimental plot. The upstream part of the ERT line is located outside of the artificial rain in an area called 'dry plot'. ERT data were acquired using an IRIS Syscal Junior system with a current measurement precision of 0.5%. The system features an internal switch-system board for 48 electrodes with 1-m inter-electrode spacing. Thus, the image resolution is expected high enough to image the global development of water infiltration and subsurface flow in the slope. Hydrological processes occurring at the centimetric scale are not detected with this electrode spacing. Three to six stacks were systematically realized for each quadrupoles in order to obtain a maximum standard deviation of 3% for the repeated measurements. Data acquisition lasted approximately 15 min; an acquisition was conducted every 1–3 h.

With respect to the low electrical noise observed on the slope, a dipole–dipole configuration was selected for its accurate resistivity value measurements (Rings and Hauk, 2009). Each acquisition includes 647 quadrupole measurements. Two acquisitions before the start of the rain experiment were conducted to characterize the initial resistivity state of the slope, and 32 acquisitions were made during the rain experiment. A filtering was applied to remove all data with a measured potential lower than 5 mV. After filtering, 87% of the original dataset was kept for the analysis. The electrical potential, the input current electrode geometry and the ERT line topography

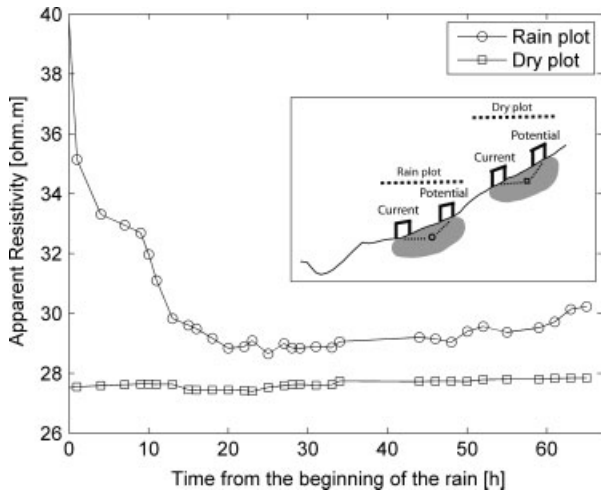


Figure 2. Example of apparent resistivity values with time for a quadrupole in the rain plot and a quadrupole in the dry plot using a dipole–dipole array. A schematic view of the quadrupole location with their integrated-volume measurement (in grey) is presented in the square

are used to compute apparent resistivity value as input to the inversion process. Figure 2 gives an example of apparent resistivity changes with time for a quadrupole centred in the rain plot and a quadrupole in the dry plot integrating large volume of soil. A decrease in apparent resistivity is observed in the rain plot, while the apparent resistivity stays nearly constant in the dry plot indicating a relative low impact of the surrounding noise level on large volume-averaged measurements. However, apparent resistivity integrating smaller volumes of soil (at shallow depths) of short-spaced quadripoles can be influenced by temperature changes. Thus, noise can be introduced in the inversion processes. Therefore, the effects of soil temperature on the resistivity values have to be estimated.

Effect of temperature on the resistivity values

To determine the effects of soil temperature on the resistivity values, soil temperature was monitored near the experimental plot along a vertical profile at different depths (–0.13, –0.30, –0.50 and –0.85 m). In addition, two temperature sensors were installed inside the rain plot at –1.90 and –2.90 m in piezometers. Figure 3 shows the temperature measurements from the beginning until the end of the rain experiment for different depths.

A small decreasing trend of soil temperature is observed during the rain experiment. Between the ground surface and –0.5 m depth, the temperature signal has a daily sine variation and varies between 14 and 8 °C. For depths below 0.5 m, the amplitudes of temperature variations are <1 °C. According to the model of thermal diffusivity with effective soil saturation of Johansen (1975), the effect of conductive heat flow due to water input can be neglected for a saturation degree of more than 25% (Behaegel et al., 2007) which is comparable to the initial soil water content in the slope. By using the model of Campbell et al. (1948) and using the soil temperature at the start of the rain experiment, the maximum relative resistivity changes in function of temperature is

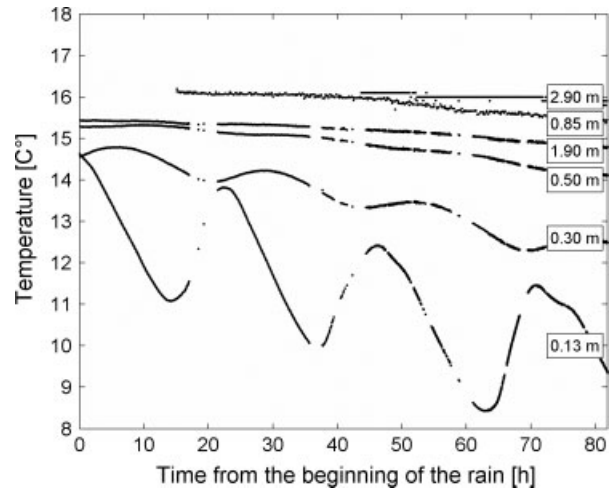


Figure 3. Temperature monitoring at different depth near the rain plot

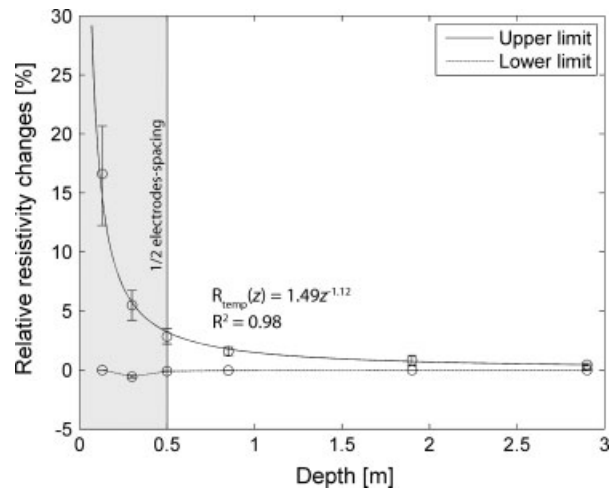


Figure 4. Maximum of relative resistivity variation caused by soil temperature changes. The maximum of relative resistivity changes are located above 0.5 m depth. Above that depth, the inverted resistivity models are poorly resolved (less than 0.5 electrode spacing)

estimated (Equation (1)).

$$\left[\frac{\rho}{\rho_{ref}} - 1 \right] \times 100 = \left[\frac{1}{1 + \alpha(T - T_{ref})} - 1 \right] \times 100(\%) \tag{1}$$

where ρ is the inverted resistivity value during the temporal monitoring corrected at temperature T_{ref} , ρ_{ref} is the inverted resistivity value at the start of the experiment, T and T_{ref} are the temperatures associated to ρ and ρ_{ref} , and α is a temperature compensation factor. The α -factor is determined empirically from measurements of different soils solutions at different temperatures. No α -factor was determined for black marls; however, it varies between 0.018 and 0.028 °C⁻¹ for natural soil (Keller and Frischknecht, 1966; Samouëlian et al., 2005; Drnevich et al., 2008; Ma et al., 2010).

At each depth of temperature sensors, the minimum and maximum of resistivity changes were used for calculating the maximum range of resistivity change in function of depth. The results for a α -factor of 0.023 °C⁻¹ ± 0.05 °C⁻¹ are indicated in Figure 4.

At shallow depths, resistivity changes are very sensitive to soil temperature changes. The temperature effects at depths below 0.5 m (corresponding to a 0.5 electrode spacing) are rapidly damped (less than 3% of resistivity variation). The relative resistivity changes due to temperature *versus* depth follow a power law (Equation (2)).

$$R_{\text{temp}}(z) = 1.49z^{-1.12} (\%) \text{ for } \alpha = 0.023 \text{ }^{\circ}\text{C}^{-1} \quad (2)$$

where z is the depth perpendicular to the topographical surface.

Equation (2) varies between two sub-equations calculated with the two extreme α -factors (Equations (3) and (4)) which determine the uncertainty of Equation (2):

$$R_{\text{temp}}(z) = 1.91z^{-1.10} (\%) \text{ for } \alpha = 0.018 \text{ }^{\circ}\text{C}^{-1} \quad (3)$$

$$R_{\text{temp}}(z) = 1.04z^{-1.18} (\%) \text{ for } \alpha = 0.028 \text{ }^{\circ}\text{C}^{-1} \quad (4)$$

These empirical equations indicate that inverted resistivity values above 0.5 m can be very noisy because of temperature changes. Correction of temperature effects will not significantly improve the results because the very shallow layers are generally poorly resolved in term of inverted resistivity values. Consequently, inverted resistivity values above 0.5 m depth are removed from the inverted models and the consequent analysis.

Approach used for time-lapse inversion

The apparent resistivity values were inverted using the time-lapse approach based on cross models implemented in the *RES2DINV* inversion software (Loke, 2006). The basic of a cross model is the use of an inverted model from a base dataset as the reference model for later datasets. Changes in subsurface resistivity are computed by using the apparent resistivity changes to ensure that changes of inverted resistivity values are only due to changes in apparent resistivity values (Loke, 1999; Miller *et al.*, 2008).

As the time-lapse inversion module of *RES2DINV* is restricted to inversion of 12 time series, the 32 datasets acquired during the rain experiments were separated into three groups. To ensure that the inversion of each group starts from the same initial model, the reference model t_{0-14h} (e.g. 14 h before the start of the rain experiment) was systematically included at the beginning of each group.

Six groups of inverted model (G1–G6) were created by varying (i) the cross model and (ii) the time-lapse inversion method. The inversion parameters presented in Table I were kept at constant values.

Three types of cross models were used. The first cross model was based on a damped least-squared Gauss-Newton algorithm to minimize the differences in the model resistivity values between the initial model and the time-lapse model (Loke, 1994). The second cross model used a least-squared smoothness constraint set to avoid sudden important changes in resistivity values. The third cross model was based on a smoothness constraint set

Table I. Inversion groups with the types of cross model and inversion parameters

	Damped least-squares constraint	Least-squares smoothness constraint	Robust smoothness constraint
Simultaneous	G1	G3	G5
Sequential	G2	G4	G6
Initial damping factor	0.1	Maximal number of iterations	8
Minimal damping factor	0.005	Vertical to horizontal regularization	1
Convergence limit	5%	Increase in damping factor with depth	1.1

minimizing the absolute changes in the model resistivity (Claerbout and Muir, 1973).

Two methods of time-lapse inversion were tested. The first method allows to inverse the datasets simultaneously. After each iteration, the inversion of the reference dataset was directly followed by the inversion of the later dataset. The second method consisted in fully inverting the datasets after a maximum of eight iterations; then the model of the last iteration of the reference dataset is used as the reference model for the later datasets.

The choice of the best inverted models was based on two statistical criteria:

1. The value of RMS error: it is the most important quantitative criteria indicating how the inverted resistivity models fit with the datasets. Inverted models with low RMS are preferred, especially those presenting the lowest RMS value for the first inverted model which is the model of reference t_{0-14h} (corresponding to the dry state conditions in the slope before the rain) used for the comparison with the later inverted models.
2. The stability through time of the inverted resistivity values observed in the dry plot of the inverted models after removing the values affected by soil temperature changes.

The sensitivity of the best inverted model was then computed with the Loke's software which gives qualitative information on how much resistivity values are constrained by the data (Loke, 2006).

To outline the changes of resistivity values with time, the difference between successive resistivity measurements are more accurate than absolute values because systematic errors are eliminated (Samouëlian *et al.*, 2005). Consequently, to track the changes to the reference model, Equation (5) was used:

$$\Delta\rho_t = 100 \frac{\rho_t - \rho_{t0}}{\rho_{t0}} (\%) \quad (5)$$

where ρ_t is the inverted resistivity value during the temporal monitoring, and ρ_{t0} is the inverted resistivity value at the reference state (t_{0-14h}).

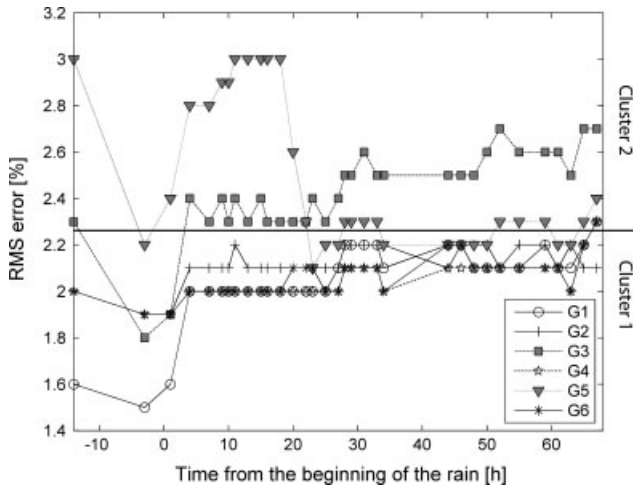


Figure 5. Changes in RMS errors for the inverted models of the six groups of cross models. Two clusters can be distinguished: cluster 1 contains the inverted models with low, stable and comparables RMS error values; cluster 2 contains the inverted models presenting higher and less stable RMS error values

RESULTS: BEST INVERTED RESISTIVITY MODELS

The first step consists in analysing the quality of the inverted models according to the criteria presented in the section on Approach used for Time-Lapse Inversion. All inversions resulted in inverted models with RMS errors smaller than 3.0%, reflecting the good quality of the input datasets (Figure 5). After five to seven iterations, the RMS remains at constant values. Two clusters of inverted models can be distinguished (Figure 5):

1. The first cluster (cluster 1) includes inverted models G1, G2, G4 and G6 characterized by stable and comparable value of RMS errors (lower than 2.2%) through time. G1 has the lowest RMS error.
2. The second cluster (cluster 2) contains the inverted models G3 and G5 displaying higher and less stable RMS errors with time.

The median value of resistivity changes is used for quantifying the global resistivity trend within the rain plot and the dry plot during the rain experiment below the depth affected by soil temperature changes (Figure 6). After about 20 h, the relative resistivity values inside the rain plot progressively decrease until - 15% of the reference state for all groups of inverted models. Observed relative changes in the dry plot are nearly null except for G5 demonstrating high variability in the dry plot. G1 has the most constant resistivity values through time in the dry plot and the lowest RMS error. After removal of the temperature effect, the residual resistivity change ($R_{residual}$) in the dry plot is about 1%.

According to the criteria presented in the section on Approach used for Time-Lapse Inversion, the inverted model G1 is used for the hydrological interpretations, especially because the initial state at t_{0-14h} displays the lowest RMS error (1.6%). As G1, G2, G4 and G6 have similar RMS errors, they are used for calculating

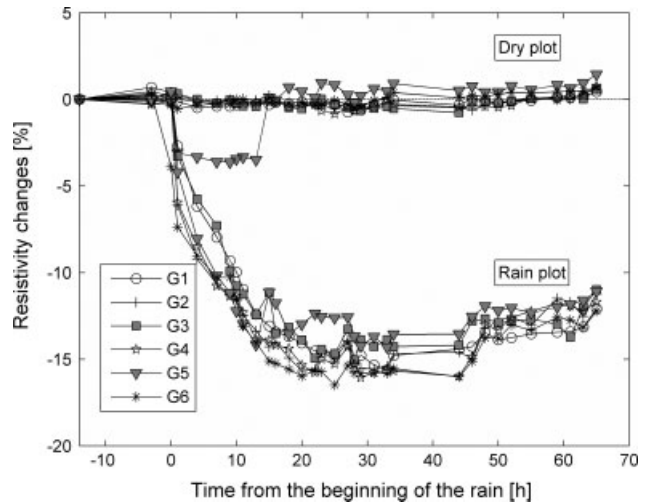


Figure 6. Inverted resistivity changes within the dry plot (149 nodes) and within the rain plot (207 nodes) for the six inversion groups

resistivity uncertainties. For this study, the uncertainty is defined by the maximum difference between the resistivity values in G1, G2, G4 and G6 at each location normalized on t_{0-14h} in G1.

Figure 7 shows the inverted resistivity values for the reference model G1 (Figure 7A), the associated uncertainty (Figure 7B) and sensitivity (Figure 7C). Resistivity values vary between 10 and 130 Ωm which are similar values to those observed in other landslides developed in black marls (Schmutz *et al.*, 2000; Grandjean *et al.*, 2007; Méric *et al.*, 2007) (Figure 6A). An upper and a lower layer can be distinguished. The limit separating these two layers is globally in good agreement with the bedrock depth deduced from dynamic penetration tests. The lower layer which displays resistivity values between 5 and 30 Ωm is the compact bedrock. The bedrock is overlaid by the weathered clay shale (e.g. landslide material) with higher resistivity values between 30 and 130 Ωm reflecting dry initial slope conditions. The largest uncertainties are mainly localized in the top of the weathered clay shale characterized by high resistivity values (>50 Ωm) and low sensitivity values.

No confidence is given to resistivity values below the interface separating the weathered clay shale from the bedrock because the sensitivity values are too low (<0.2%). Consequently, this interface is assumed to represent the maximal investigation depth of the ERT.

HYDROLOGICAL INTERPRETATIONS

Steady-state flow conditions

Steady-state flow refers to the condition where the fluid properties at any single point in the slope system do not change over time, and to the conditions of no possibility of additional storage of water in the soil. When relative resistivity values reach a threshold value, parameters affecting resistivity values (e.g. water chemistry, soil compaction, water saturation and clay content) are balanced or constant. To determine the

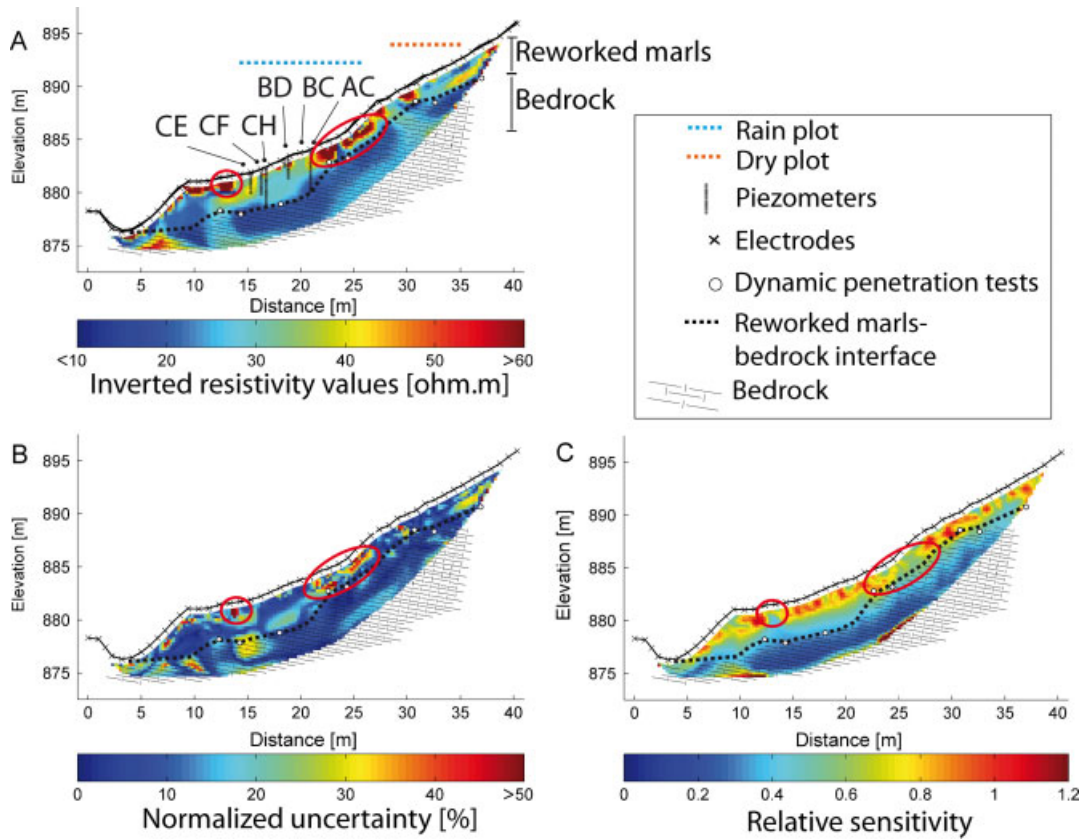


Figure 7. (A) Inverted resistivity model of the G1 reference (t_{0-14h}) acquired before the start of the rain. (B) Uncertainty defined by the maximum and the minimum of the inverted resistivity values in the inverted models G1, G2, G4 and G6 normalized with G1. (C) Associated sensitivity index of G1. The red circles indicate areas with high uncertainty and low sensitivity index

time at any locations inside the experimental plot when constant resistivity value occurs, an automatic routine based on the uncertainty level in the inverted resistivity model G1 relative to the reference model (t_{0-14h}) is developed.

Considering the effect of soil temperature discussed in the section on Effect of Temperature on the Resistivity Values, the relative uncertainty induced by soil temperature changes ($R_{temp} = \Delta\rho/\rho_{t0}$) can be separated from the total relative uncertainty (R_{total}). As a consequence, R_{total} can be expressed by Equation (6):

$$R_{total} = R_{temp} + R_{residual} \quad (6)$$

If we assume that $R_{residual}$ is constant and similar to the value observed in the dry plot after removal of the effects of soil temperature, it is possible to define R_{total} as a function of depth using Equation (7):

$$R_{total}(z) = 1.49z^{-1.12} + 1 \quad (\%) \quad (7)$$

where z is the depth perpendicular to the topographical surface.

When the standard deviation of the relative resistivity is less than R_{total} during 24 h, no significant change is assumed to have occurred and a constant level of relative resistivity value is reached. To obtain values every hour, a piecewise linear interpolation technique is applied at each location. Thus, the time of constant resistivity

value is computed for each cell of the ERT dataset. Equations (3) and (4) are used to calculate the error on the time by introducing the term R_{temp} in Equation (6).

The results and the associated errors are detailed in Figure 8A and B. The time of constant relative resistivity value is then compared with the time of constant ground water level observed in some piezometers (Figure 9A and B). A good match is found except for piezometer BC, as this piezometer is installed in a block of marls which is too small to be imaged with our ERT resolution (electrode spacing of 1 m). The reliability of this matching is also confirmed by the hydrochemical observations of Garel *et al.* (2011) which indicate that subsurface water flow is predominant after 20 ± 2 h and that the soil could be considered very close to saturation at this time. From these statements, the times determined from ERT data are linked to the times of steady-state flow conditions. Therefore, interpretation of resistivity changes is thus possible in term of water saturation assuming water salinity, porosity and soil structure constant with time.

On average, times of steady-state flows conditions are reached 21 h after the start of the rain. The topsoil is characterized by relatively short times varying between 5 and 15 ± 1 h, while deeper locations mostly reached steady-state flow conditions after $20-28 \pm 1$ h. More time is needed for locations downstream outside the rain plot ($30-35 \pm 5$ h) to reach steady-state conditions. This time difference between area outside and inside the rain

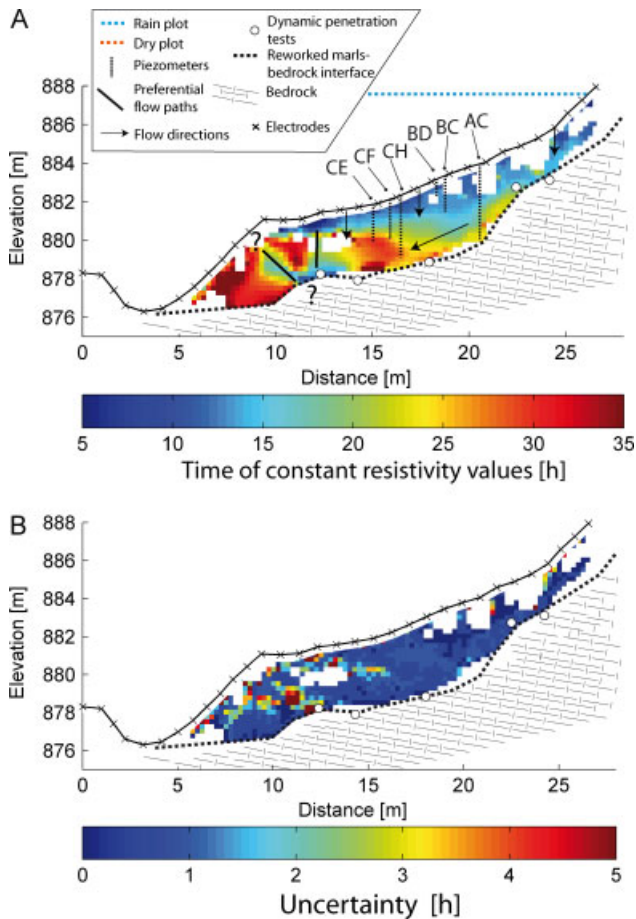


Figure 8. (A) Times of constant resistivity values. Two preferential flow paths are suspected near the landslide toe. The development of a subsurface lateral flow inside the rain plot in depth is also suspected. (B) Uncertainty associated to the identification of time of steady-state conditions

plot strongly suggests the development of subsurface lateral flow during the rain experiment (Figure 8A).

Two preferential flow paths could be detected near the abrupt change of slope delimiting the landslide toe from the other part of the landslide body (Figure 8A). These flow paths induce fast water infiltration until the weathered clay shale/bedrock interface thus leading to steady-state conditions after a short time of rain experiment ($ca\ 15 \pm 2$ h). These preferential flows are probably connected through the weathered clay-shale/bedrock interface. However, their location and geometry inside the bedrock cannot be detected because of too low sensitivity value of the inverted model.

Hydrological interpretation of the resistivity changes

A lack of independent soil moisture measurements impeded establishing a reliable relationship among resistivity values and soil moisture values. However, regarding the conclusions of section Steady-State Flow Conditions, changes in soil water content seem the most predominant factor affecting resistivity changes in this type of weathered clay shale thus making the influence on other factors such as water salinity, soil porosity and clay content negligible for qualitative interpretation. Figure 10

presents the time-lapse of the resistivity changes with the associated uncertainty. Except at the time t_{0+1h} , the resistivity changes are significant enough regarding the uncertainties. A decrease in resistivity (e.g. negative anomaly) is observed with time following directly the onset of the rain. This observation reflects the development of a wetting front progressing mainly vertically during the first 10 h of the experiment. The area located downstream and outside of the rain plot is then affected by a negative anomaly showing that a lateral subsurface flow is developing. After 30 h of rain, this lateral subsurface flow may have reached the Laval stream. The evolution below the weathered clay-shale/bedrock interface is not indicated because the sensitivity is too low below it. Consequently, infiltration inside the bedrock cannot be depicted from the ERT dataset. However, regarding the lateral development of the subsurface water flow at about t_{0+20h} when the entire rain plot is in steady-flow conditions, an important permeability contrast between the weathered clay-shale and the bedrock can be suspected.

Conceptual hydrological model

On the basis of the time evolution of resistivity changes and the location of steady-state flow conditions inside the rain plot, a conceptual hydrological model is proposed. The wetting front is estimated by the isovalue of -5% of resistivity change (Figure 11).

- t_0-t_{0+5h} : in the first hours of the rain experiment, the wetting front has already penetrated the first meter of the top soil. The preferential flow paths located near the landslide toe allow water to reach rapidly the bedrock interface;
- $t_{0+5h}-t_{0+12h}$: vertical water infiltration is still dominant. Steady-state flow conditions are reached in the top-soil. Consequently, the groundwater level observed in piezometer BD stays at its maximal level. In the deepest piezometers CH and AC, the ground water levels start to progressively rise. At the same time, water infiltration occurs on the top of the landslide toe, probably supplied by surface water runoff coming from the rain plot. In that area, the preferential flow paths are still draining water until the bedrock depth where steady-flow conditions are progressively reached. The wetting front starts infiltrating downslope showing the formation of subsurface lateral flow draining water outside of the rain plot;
- $t_{0+12h}-t_{0+15h}$: inside the rain plot, steady-state flow conditions are progressing faster in depth than outside the rain plot. The wetting front reaches the bedrock interface;
- $t_{0+15h}-t_{0+20h}$: the surrounding of the preferential flow paths progressively entered in steady-state flow conditions and could be considered as very close to saturation. Consequently, subsurface lateral flow starts its progression inside the landslide toe. Surface water runoff contributes also to infiltrate water in the toe;

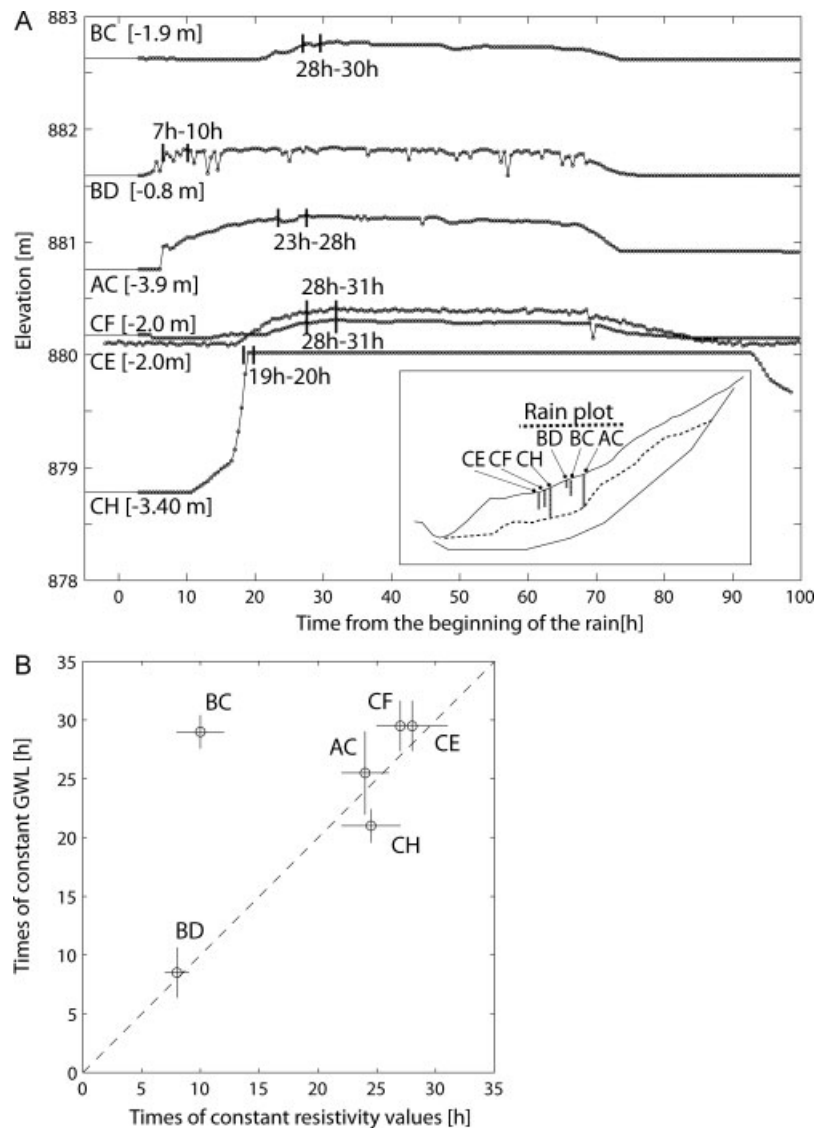


Figure 9. (A) Ground water level changes in piezometers located along the ERT line. After a certain time the groundwater level remains constant until the end of the rain experiment. [\times m] is the piezometer depth. (B) Comparison with the time of constant resistivity values with the time of constant ground water level observed in the piezometers

- $t_{0+20h} - t_{0+25h}$: the entire rain plot is in steady-state flow conditions. Ground water levels remain at a constant level in nearly all piezometers;
- $t_{0+25h} - t_{0+30h}$: the subsurface lateral flow may have connected the Laval stream. Steady-state flow conditions are reached both in the landslide toe and in the rain plot.

DISCUSSION

ERT acquisitions

Considering the objectives of the study, the spatial and temporal resolution of the ERT dataset was large enough to monitor the general evolution of the infiltrated water. The fixed acquisition time of 15 min for a single ERT acquisition obviously integrated all the hydrological processes occurring within this lapse of time. Nevertheless, this time of acquisition with a frequency of 1–3 h was suitable for monitoring the global development of

the infiltrated water before the soil reached steady-state flow conditions. Improvement in more frequent and faster acquisition devices would help for increasing the temporal resolution. At the same time, an increase in the number of electrodes along the surface (thus reducing the electrode spacing) is necessary to improve the spatial resolution of time-lapse ERT inversion both for shallow depths (first half meter) and deeper depths (Descloitres *et al.*, 2007; Clément *et al.*, 2009).

Uncertainties of the inverted resistivity values

In this article, the uncertainty estimations were based on the maximum difference between resistivity values from four inverted models with similar RMS errors. The temporal stability of apparent and inverted resistivity values in a test site was also shown to be a good method to estimate the uncertainty in resistivity changes. Some analysis for estimating the error in the measured data affecting inversion quality could be also considered in

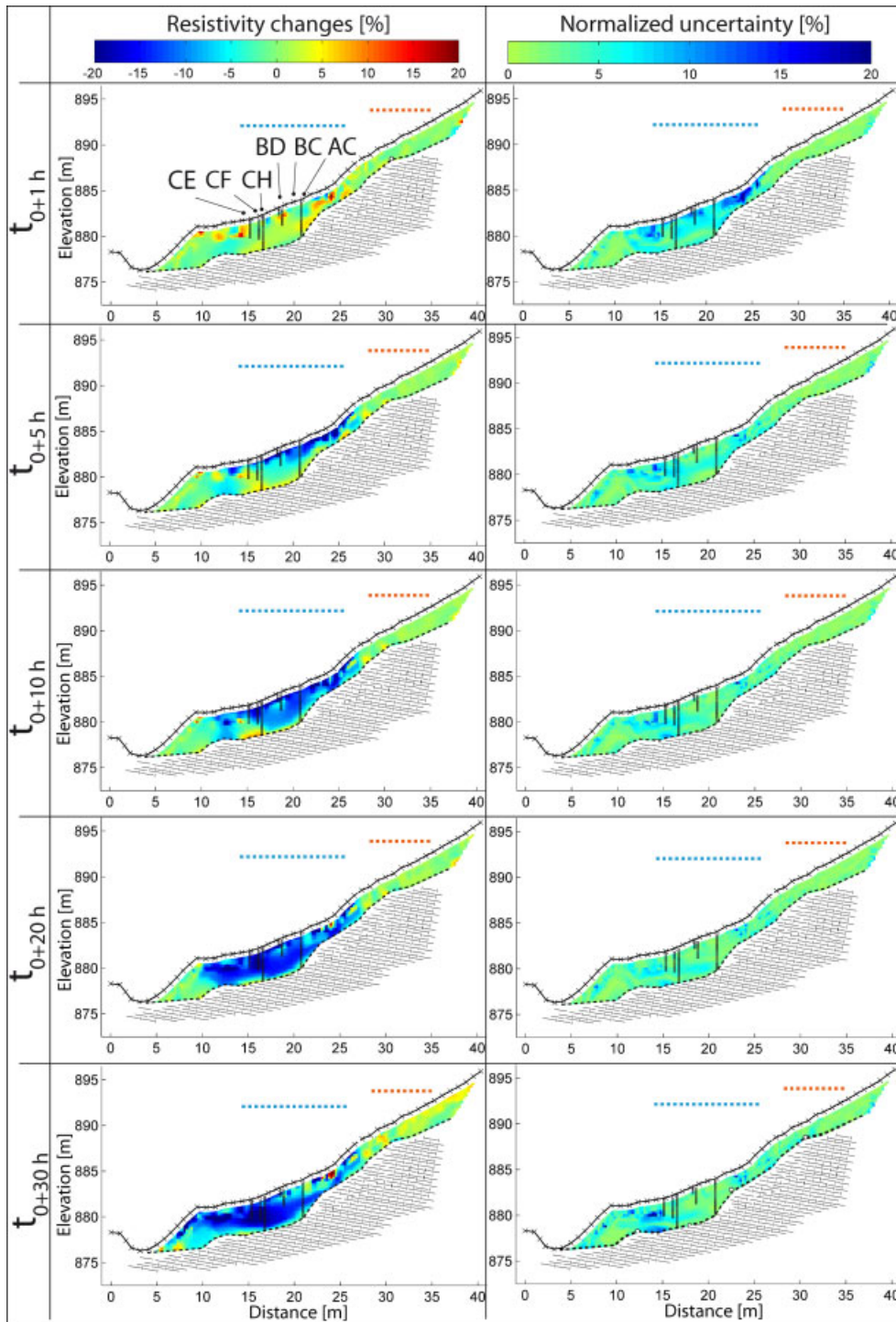


Figure 10. Resistivity changes during the rain experiment with the associated uncertainty. The development of subsurface lateral flows can be highlighted. See Figure 8 for the legend

the future (surrounding noise, suitability of acquisition configurations and error in electrode locations). For example, Jelinkova *et al.* (2006) were able to image infiltration processes during infiltration experiment, but they pointed out developments of inconsistencies linked to the design and the scale of the ERT. The effects of these different factors can be estimate with numerical modelling (Descloitres *et al.*, 2007) or with systematic tests during the acquisition. Indeed, normal and reciprocal measurements would help to measure the noise directly

in the electrical potential values in future experiment (LaBrecque *et al.*, 1990). To avoid uncertainties due to measurement errors of electrode spacing, the difference in measured potential can also be used in the inversion process.

In such type of rain experiments on steep slopes with significant clay fraction and possible soil deformation (Fukue *et al.*, 1999), interpretation of inverted resistivity can be rather complex. In this study, soil deformation monitoring with terrestrial laser scanning did not show

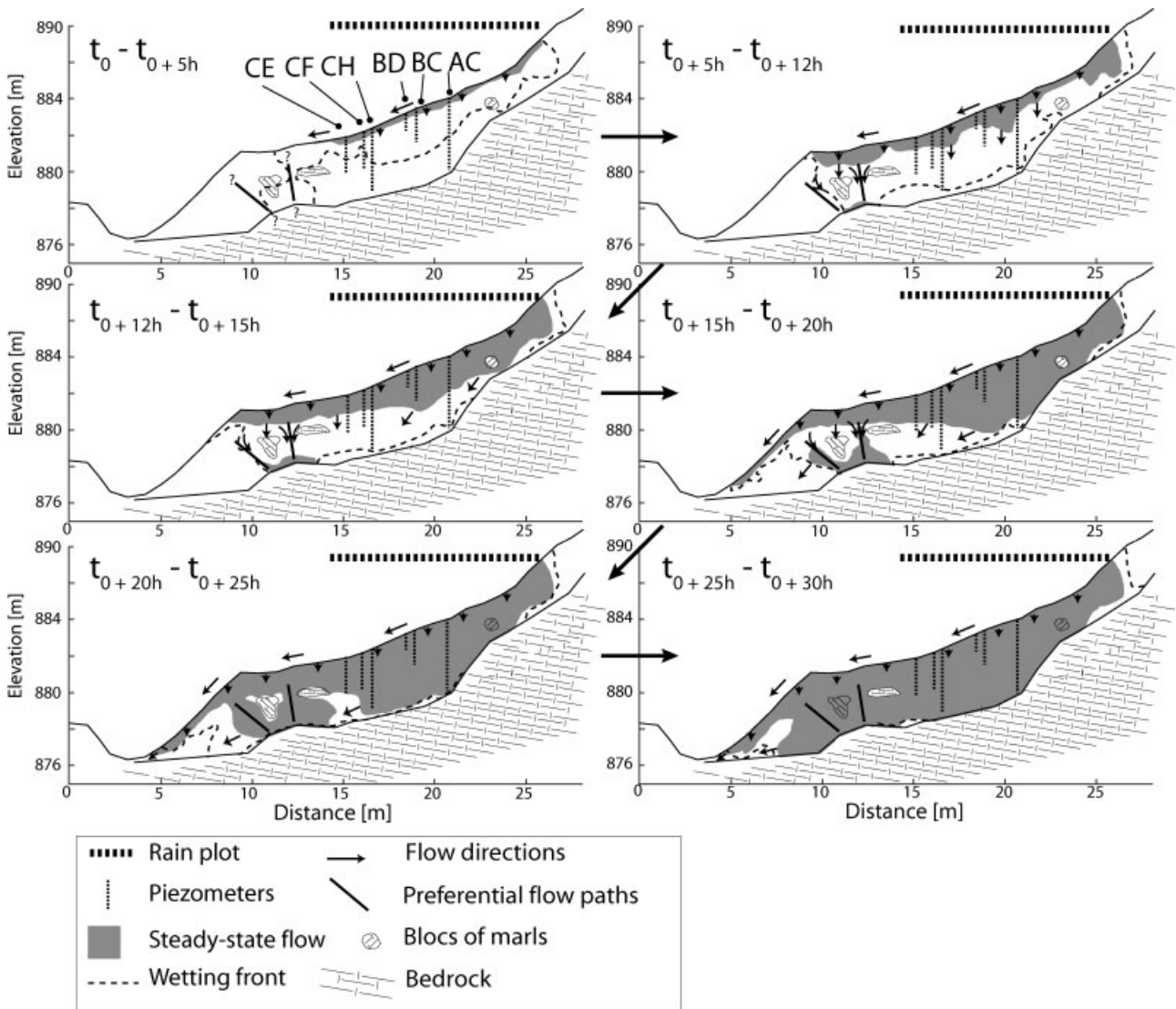


Figure 11. Hydrological concept of water infiltration during the rain experiment. In the first hours, vertical infiltration is dominant, then lateral subsurface flows is developing along the landslide material–bedrock interface. Two preferential flow paths near the landslide toe allow water to reach the bedrock in a short time after the beginning of the rain. Areas characterized with higher times of steady-state flow conditions are identified as marly blocks

any evidence of compaction or displacements that could lead to a change in soil structure. Therefore, the effect of that factor on the resistivity values was assumed negligible. Another important factor is the resistivity of the rain water. Globally, the conductivity of the rain input was one order of magnitude lower than the conductivity of the pre-event water already present in the soil before the start of the rain. The experiment started from unsaturated condition (about 27% of saturation) and a decrease in resistivity directly occurred after the beginning of the rain (Figures 6 and 10). Regarding the model of Waxman and Smits (1968) for clay-shale sands, an increase in water saturation is the only way to produce such a resistivity response assuming constant porosity (no change in soil structure) and conductivity along clay surfaces. In other words, these observations imply that the resistive rain water input had a lower effect on the resistivity values than a change in degree of water

saturation for this type of weathered clay-shale slope in initial unsaturated conditions.

Comparison between inverted resistivity and soil moisture measurements

The problem of measurements scalability of representative volumes between inverted resistivity values (meter-scale) and soil moisture from TDR (Time-Domain Reflectometer) measurement (cm-scale) is often pointed out as a main problem for comparing inverted resistivity and soil moisture measurements (Schwartz *et al.*, 2008). Three-dimensional effects induced by lateral water drainage and infiltration can also impede the inversion of accurate resistivity values (Spitzer, 1998; Wisen *et al.*, 2003).

For this study, two main reasons explained the difficulty of finding a reliable relationship between volumetric soil moisture and inverted resistivity values.

1. The first reason is due to the non-uniqueness of the inverted model inducing variability in the inverted

resistivity at some shallow locations where the TDR are installed (Figure 1C). A reliable quantification of the true values of resistivity is still very difficult as already demonstrated by Rings and Hauk (2009). This problem was often illustrated by many authors if no additional constraints are imposed in the boundary conditions (Olayinka and Yaramanci, 2000; Bemberger *et al.*, 2008; Koestel *et al.*, 2008). Therefore, introducing additional knowledge in the inversion procedure like bedrock depth or areas with known resistivity values would help to reduce the non-uniqueness of the model (Loke, 2006).

2. The second reason results from an insufficient range of soil moisture and resistivity values at the location of the TDR. For illustrating the problem, Figure 12 shows the relationship between resistivity and calibrated soil water content for different clay-rich soils obtained from laboratory experiments (McCarter, 1984; Fukue *et al.*, 1999; Michot *et al.*, 2003) presented in Samouëlian *et al.* (2005). These values are plotted with the inverted resistivity values calculated for the weathered black marls of the Laval landslide. The horizontal error bars of water content values and resistivity values are based on the method exposed in the section on Result: Best Inverted Resistivity Models. The uncertainty on the true inverted resistivity is too large to adjust a trendline. Regarding the trend observed in clay-rich soils from the laboratory experiments, volumetric water contents of less than 20% associated with higher resistivity values would help to fit a reliable law. More soil moisture measurement at different depths and locations along the ERT profile would help to extent the range of soil moisture and resistivity values in future rain experiments.

Hydraulic conductivity

The inverse of the gradient of steady-state times (∇ Time in h m^{-1}) can be used to estimate an apparent saturated hydraulic conductivity K_s . ∇ Time is determined along two profiles P1 and P2 parallel to the subsurface

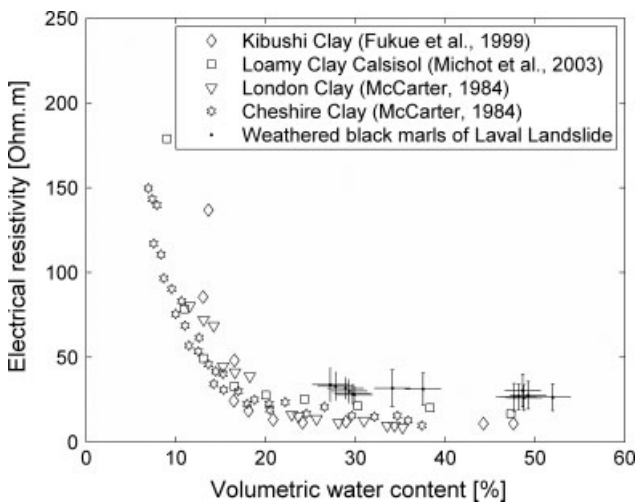


Figure 12. Relationship between electrical resistivity values and volumetric water content for clay-rich soils

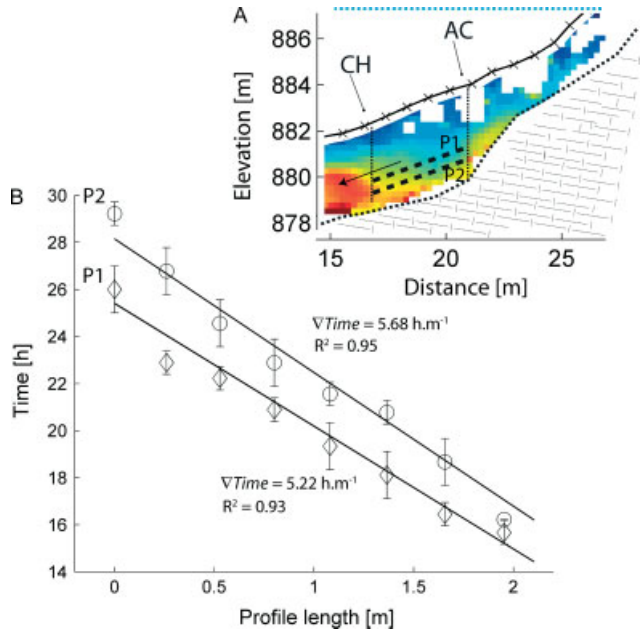


Figure 13. Estimation of the apparent saturated hydraulic conductivity on two profiles parallel to the subsurface lateral flow (A) Location of the profiles P1 and P2 between the piezometers CH and AC in Figure 8A. See Figure 8A for the legend. (B) Estimation of for the profiles P1 and P2

flow direction (Figure 13A and B). The mean hydraulic charge (i) is given by the measured groundwater levels observed in piezometers AC and CH (Figures 9A and 13A). Darcian flow, continuous water table and homogeneous soil are assumed between the piezometers. K_s can thus be determined with Equation (8):

$$K_s = \frac{1}{3600 \nabla \text{Time}} i (\text{m s}^{-1}) \quad (8)$$

Regarding the gradient ∇ Time of P1 and P2, an average K_s of $1.7 \times 10^{-4} \text{ m s}^{-1}$ is obtained. This value is comparable with values of K_s measured from constant head permeameters measurements realized on soil samples as well as *in situ* inverse auger tests carried out in the piezometers AC and CH (K_s of $4.9 \times 10^{-5} \text{ m s}^{-1}$; Garel *et al.*, 2011). This relatively high apparent saturated hydraulic conductivity shows how fast the soil is draining the infiltrated water as soon as steady-state conditions are reached.

CONCLUSION

This study has demonstrated the high potential of ERT for monitoring water infiltration during rain experiments. Time-lapse ERT combined to hydrological investigations allowed to determine water flows circulating inside the clay-shale slope of the Laval landslide. ERT could provide a continuous image of the main hydrological processes occurring within the soil by integrating information on large volume. The conceptual hydrological model derived from the ERT cannot obviously explain complex hydrological behaviour suggested by discrete

information from hydrological and hydrochemical methods (e.g. isolated water at small scale with no connection with the surrounding; Garel *et al.*, 2011). However, the main processes occurring at larger scale are highlighted. Regarding the initial conditions of the experiment, 21 h of rainfall were necessary to reach the maximal capacity of water storage of the soil. At that time, subsurface lateral flow rate and surface runoff rate were maximal. The analyses of time-lapse ERT as well as calculated saturated hydraulic conductivities demonstrate the potential of the weathered soil to rapidly drain the infiltrated water towards the Laval stream. These conclusions are in agreement with hydrological measurements (chemical tracing and ground water level monitoring).

Structural information is also examined. The bedrock depth could be derived from the ERT and is consistent with dynamic penetration tests. Preferential flow paths could also be suspected near the landslide toe indicating possible presence of extension fissures or a more permeable matrix. However, a complete quantitative interpretation of ERT could not be achieved because of several limitations related to the non-uniqueness of the inverted models and to the difficulty of linking inverted resistivity value with TDR measurements with an acceptable accuracy.

Coupling 3-D ERT at the ground surface and cross holes ERT measurements with short acquisition time would help for providing 3-D interpretation of subsurface water flows and minimizing possible 3-D effects. Reproducing similar rainfall experiences with different intensities and slope conditions could provide complementary and valuable information on subsurface flow development in weathered clay-shale slopes.

ACKNOWLEDGEMENTS

This work was supported by the European Commission within the Marie Curie Research and Training Network 'Mountain Risks: from prediction to management and governance' (2007-2010, Contract MCRTN-035798) and by the French National Research Agency (ANR) within the project 'Ecou-Pref -Ecoulements préférentiels dans les versants marneux' (Contract ANR05-ECCO-007-04). The authors would like to acknowledge Emilie Garel, Christophe Emblanch and Anne-Laure Cognard-Plancq (University of Avignon and Pays de Vaucluse), Nicole Mathys and Sébastien Klotz (Cemagref), Olivier Maquaire and Matthieu Fressard (University of Caen-Basse-Normandie), Mathieu François (BRGM) and Dominika Krezminska (Delft University of Technology) who participated to the data acquisition on the field. The authors thank Karen Sudmeier-Rieux Sluyter (University of Lausanne) for improving the English of this article. The authors are also grateful to two anonymous reviewers for their help in considerably improving the manuscript.

REFERENCES

- Antoine P, Giraud D, Meunier M, Van Ash T. 1995. Geological and geotechnical properties of the "Terres Noires" in southeastern France: weathering, erosion, solid transport and instability. *Engineering Geology* **40**: 223–234.
- Archie GE. 1942. The electrical resistivity log as an aid in determining some reservoir characteristics. *Transaction of American Institute of Mining, Metallurgical, and Petroleum Engineers* **146**: 54–62.
- Barker R, Moore J. 1998. The application of time-lapse electrical tomography in groundwater studies. *The Leading Edge* **17**: 1454–1458.
- Behaegel M, SAILHAC P, MARQUIS G. 2007. On the use of surface and ground temperature data to recover soil water content information. *Journal of Applied Geophysics* **62**: 234–243.
- Bemberger E, Furman A, Linker R. 2008. Using vadose zone flow model data in ERT inversion for improved estimation of water content distribution. American Geophysical Union, Fall Meeting, San Francisco, abstract H44C-03.
- Binley A, Henry-Poulter S, Shaw B. 1996. Examination of solute transport in an undisturbed soil column using electrical resistance tomography. *Water Resources Research* **32**: 763–769.
- Campbell RB, Bower CA, Richards LA. 1948. Change of electrical conductivity with temperature and the relation of osmotic pressure to electrical conductivity and ion concentration for soil extracts. *Soil Science Society of America Journal* **13(C)**: 66–69. DOI: 10.2136/sssaj1949.036159950013000C0010x.
- Claerbout JF, Muir F. 1973. Robust modeling with erratic data. *Geophysics* **38**: 826–844.
- Clément R, Descloitres M, Günther T, Ribolzi O, Legchenko A. 2009. Influence of shallow infiltration on time-lapse ERT. Experience of advanced interpretation. *C. R. Geoscience*. DOI: 10.1016/j.crte.2009.07.005.
- Corona C, Robert Y, Rovera G. 2002. Suivi de l'érosion et modélisation des vitesses de déplacement des sédiments sur versants marneux très de'gradés. Application sur les badlands de Draix grâce au topomètre laser photographique. In *Geomorphology: From Expert Opinion to Modelling*. ECGH, Delahaye D, Levoy F, Maquaire O (eds). Strasbourg; 177–184.
- Cras A, Marc V, Travi Y. 2007. Hydrological behaviour of sub-Mediterranean alpine headwater streams in a badlands environment. *Journal of Hydrology* **339**: 130–144.
- Daily W, Ramirez A, Labrecque D, Nitao J. 1992. Electrical resistivity tomography of vadose water movement. *Water Resources Research* **28(5)**: 1429–1442.
- Descroix L, Olivry JC. 2002. Spatial and temporal factors of erosion by water of black marl in the badlands of the French Southern Alps. *Hydrological Sciences Journal* **47(2)**: 227–242.
- Descloitres M, Ruiz L, Sekhar M, Legchenko A, Braun J-J, Kumar MSM, Subramanian S. 2007. Characterization of seasonal local recharge using electrical resistivity tomography and magnetic resonance sounding. *Hydrological Processes* **22**: 384–394.
- Drnevich VP, Zambrano CE, Jung S, Clarke JP. 2008. Electrical conductivity of soils and soil properties. In *GeoCongress 2008: Characterization, Monitoring, and Modeling of GeoSystems*, Alshawabkeh A, Reddy KR, Khire MV (eds). Geotechnical special publication No. 179 of the American Society of Civil Engineers: New Orleans; 317–323.
- Estèves M, Descroix L, Mathys N, Lapetite JM. 2005. Soil hydraulic properties in a marly gully catchment (Draix, France). *Catena* **63**: 282–298.
- French H, Binley A. 2004. Snowmelt infiltration: monitoring temporal and spatial variability using time-lapse electrical resistivity. *Journal of Hydrology* **297**: 174–186.
- French H, Hardbatt C, Binley A, Winship P, Jakobsen L. 2002. Monitoring snowmelt induced unsaturated flow and transport using electrical resistivity tomography. *Journal of Hydrology* **267**: 273–284.
- Fressard M, Maquaire O, Malet J-P, Klotz S, Grandjean G. 2009. Morpho-structure and triggering conditions of the Laval landslide developed in clay-shales, Draix catchment (South French Alps). In *Proceedings of the International Conference 'Landslide Processes: from geomorphologic mapping to dynamic modelling'*, Malet J-P, Rémaitre A, Bogaard T.A. (eds). CERG Editions: Strasbourg; 107–110.
- Fukue M, Minatoa T, Horibe H, Taya N. 1999. The microstructure of clay given by resistivity measurements. *Engineering Geology* **54**: 43–53.
- Garel E, Marc V, Ruy S, Cognard-Plancq A-L, Emblanch C, Klotz S. 2011. Hydrological and hydro chemical processes observed during large scale infiltration experiment in initial unsaturated conditions: the Laval soil slope experiment. *Hydrological Processes*.

- Glover PWJ, Hole MJ, Pous J. 2000. A modified Archie's law for two conducting phases. *Earth and Planetary Science Letters* **180**: 369–383.
- Grandjean G, Hibert C, Mathieu F, Garel E, Malet J-P. 2009. Monitoring water flow in a clay-shale hillslope from geophysical data fusion based on a fuzzy logic approach. *C.R. Geoscience*. DOI: 10.1016/j.crte.2009.08.003.
- Grandjean G, Malet J-P, Bitri A, Méric O. 2007. Geophysical data fusion by fuzzy logic for imaging the mechanical behaviour of mudslides. *Bulletin de la Société Géologique de France* **2**: 127–136.
- Jelinkova V, Votrubova J, Sanda M, Císlarova M. 2006. Monitoring preferential flow during infiltration experiments. American Geophysical Union, Fall Meeting, San Francisco, abstract H31B-1419.
- Johansen O. 1975. Thermal conductivity of soils. PhD thesis, University of Trondheim; 236.
- Jongmans D, Garambois S. 2007. Geophysical investigation of landslides: a review. *Bulletin de la Société Géologique de France* **2**: 101–112.
- Keller GV, Frischknecht FC. 1966. *Electrical Methods in Geophysical Prospecting*. Pergamon Press: Oxford; 517.
- Koestel J, Kemna A, Javaux M, Binley A, Vereecken H. 2008. Quantitative imaging of solute transport in an unsaturated and undisturbed soil monolith with 3-D ERT and TDR. *Water Resources Research* **44**: DOI: 10.1029/2007WR006755.
- LaBrecque D, Ward SH. 1990. Two-dimensional cross-borehole resistivity model fitting. In *Geotechnical and Environmental Geophysics*, Ward SH (eds). Society of Exploration Geophysicists: Tulsa, OK; 51–74.
- Loke MH. 1994. The inversion of two-dimensional resistivity data. PhD thesis, University of Birmingham, Birmingham; 122.
- Loke MH. 1999. Time-lapse resistivity imaging inversion. In *Proceedings of the 5th Meeting of the Environmental and Engineering Geophysical Society European Section, European Section, Em1*, Budapest.
- Loke MH. 2006. RES2DINV ver. 3.55, Rapid 2D resistivity & IP inversion using the least-squares method. Software Manual; 139.
- Ma R, McBratney A, Whelan B, Minasny B, Short M. 2010. Comparing temperature correction models for soil electrical conductivity measurement. *Precision Agriculture*. DOI: 10.1007/s11119-009-9156-7.
- Malet J-P, Auzet A-V, Maquaire O, Ambroise B, Descroix L, Estèves M, Vandervaere J-P, Truchet E. 2003. Investigating the influence of soil surface features on infiltration on marly hillslopes. Application to callovo-oxfordian black marls slopes in the Barcelonnette basin (Alpes-de-Haute-Provence, France). *Earth Surface Processes and Landforms* **28**(5): 547–564.
- Malet J-P, Maquaire O, Hantz D, van Westen CJ, Penà-Rincon GI. 2011. Control of regolith depths on water storage capacity and slope stability in clay-shale landscapes. *Hydrological processes*.
- Maquaire O, Malet J-P, Remaître A, Locat J, Klotz S, Guillon J. 2003. Instability conditions of marly hillslopes: towards landsliding or gullyng? The case of the Barcelonnette Basin, South East France. *Engineering Geology* **70**: 109–130.
- Marescot L, Monnet R, Chapellier D. 2008. Resistivity and induced polarization surveys for slope instability studies in the Swiss Alps. *Engineering Geology* **98**: 18–28.
- Mathys N, Brochot S, Meunier M, Richard D. 2003a. Erosion quantification in the small marly experimental catchments of Draix (Alpes de Haute Provence, France). Calibration of the ETC rainfall-runoff-erosion model. *Catena* **50**(2–4): 527–548.
- Mathys N, Richard D, Grésillon J-M. 2003b. Non-linearity in erosion response of a small mountainous and marly basin: the Laval in the Draix experimental catchments, South East, France. In *International Conference. Hydrology of the Mediterranean and semi-arid regions*, Montpellier, France. CD-rom.
- McCarter WJ. 1984. The electrical resistivity characteristics of compacted clays. *Geotechnique* **34**: 263–267.
- Méric O, Garambois S, Malet J-P, Cadet H, Guéguen P, Jongmans D. 2007. Seismic noise-based methods for soft-rock landslide characterization. *Bulletin de la Société Géologique de France* **2**: 137–148.
- Michot D, Benderitter Y, Dorigny A, Nicoullaud B, King D, Tabbagh A. 2003. Spatial and temporal monitoring of soil water content with an irrigated corn crop cover using electrical resistivity tomography. *Water Resources Research* **39**: 1138.
- Miller CR, Routh PS, Broster TR, McNamara JP. 2008. Application of time-lapse ERT imaging to watershed characterization. *Geophysics* **73**: 3–17.
- Nguyen F, Kemna A. 2005. Strategies for time-lapse electrical resistivity inversion. In *Extended Abstracts of the 11th European Meeting of Environmental and Engineering Geophysics*, Palermo, Italy, 5–8 September 2005, paper A005, 4. CD ROM edition.
- Olayinka AI, Yaramanci U. 2000. Assessment of the reliability of 2D inversion of apparent resistivity data. *Geophysical Prospecting* **48**: 293–316.
- Olsen PA. 1999. Estimation and scaling of the near-saturated hydraulic conductivity. *Nordic Association for Hydrology, Lyngby, Denmark (1970–2007)* **30**: 177–190.
- Oostwoud Wijdenes DJ, Ergenzinger P. 1998. Erosion and sediment transport on steep marly hillslopes, Draix, Haute-Provence, France: an experimental field study. *Catena* **33**(3–4): 179–200.
- Rings J, Hauk C. 2009. Reliability of resistivity quantification for shallow subsurface water processes. *Journal of Applied Geophysics* **68**: 404–416.
- Robinson DA, Binley A, Crook N, Day-Lewis FD, Ferré TPA, Grauch VJS, Knight R, Knoll M, Lakshmi V, Miller R, Nyquist J, Pellerin L, Singha K, Slater L. 2008. Advancing process-based watershed hydrological research using near-surface geophysics: a vision for, and review of, electrical and magnetic geophysical methods. *Hydrological Processes* **22**: 3604–3635.
- Samouëlian A, Cousin I, Tabbagh A, Bruand A, Richard G. 2005. Electrical resistivity survey in soil science: a review. *Soil & Tillage Research* **83**: 173–193.
- Schmutz M, Albouy Y, Guérin R, Maquaire O, Vassal J, Schott J-J, Descloitres M. 2000. Joint electrical and time domain electromagnetism (TDEM) data inversion applied to the Super-Sauze earthflow (France). *Surveys in Geophysics* **4**: 371–390.
- Schwartz BF, Schreiber EM, Yan T. 2008. Quantifying field-scale soil moisture using electrical resistivity imaging. *Journal of Hydrology* **362**: 234–246.
- Sen PN, Godde PA, Sibbit A. 1988. Electrical conduction in clay bearing sandstones at low and high salinities. *Journal of Applied Geophysics* **63**: 4832–4840.
- Shah PH, Singh DN. 2005. Generalized Archie's law for estimation of soil electrical conductivity. *Journal of ASTM International* **2**(5): 1–20.
- Slater L, Binley A, Daily W, Johnson R. 2000. Cross-hole electrical imaging of a controlled saline tracer injection. *Journal of Applied Geophysics* **44**: 85–102.
- Spitzer K. 1998. The three-dimensional DC sensitivity for surface and subsurface sources. *Geophysical Journal International* **137**: 736–746.
- Waxman MM, Smits LJM. 1968. Electrical conductivity in oil-bearing shaly sand. *Society of Petroleum Engineers Journal* **8**: 107–122.
- Winship P, Binley A, Gomez D. 2006. Flow and transport in the unsaturated Sherwood sandstone: characterization using cross-borehole geophysical methods. In *Fluid Flow and Solute Movement in Sandstones: The Onshore UK Permo-Triassic Red Bed Sequence*, Barker RD, Tellam JH (eds). Geological Society of London: London; 219–231.
- Wisén R, Christiansen AV, Auken E, Dahlin T. 2003. Application of 2D laterally constrained inversion and 2D smooth inversion of CVES resistivity data in a slope stability investigation. In *Proceedings of the 9th Meeting Environmental Engineering Geophysics*. EAGE Publications: Prague, Czech Republic, Paper O-002.